An Activity Catalogue of Southern Stars

J.S. Jenkins[1], H.R.A. Jones[1], C.G. Tinney[2], R.P. Butler[3],
C. McCarthy[4], G.W. Marcy[4,5], D.J. Pinfield[1], B.D. Carter[6], A.J. Penny[7,8,9]

[1] *Centre for Astrophysics Research, University of Hertfordshire, College Lane, Hatfield, Hertfordshire AL10 9AB, email: jsj@star.herts.ac.uk*
[2] *Anglo-Australian Observatory, PO Box 296, Epping, NSW 1710, Australia*
[3] *Carnegie Institute of Washington, Department of Terrestrial Magnetism, 5241 Broad Branch Road NW, Washington, DC 20015-1305*
[4] *Department of Physics and Astronomy, San Fransisco State University, San Fransisco, CA 94132*
[5] *Department of Astronomy, University of California, Berkeley, CA 94720*
[6] *Faculty of Sciences, University of Southern Queensland, Toowoomba, 4350, Australia*
[7] *Rutherford Appleton Laboratory, Chilton, Didcot, Oxon, OX11 0QX, UK*
[8] *SETI Institute, 515 North Whisman Road, Mountian View, CA 94043*
[9] *Harvard-Smithsonian Center for Astrophysics, 60 Garden St, MA 02138,USA*

Draft: 05/05

ABSTRACT

We have acquired high-resolution echelle spectra of 225 F6-M5 type stars in the southern hemisphere. The stars are targets or candidates to be targets for the Anglo-Australian Planet Search. CaII HK line cores were used to derive activity indices for all of these objects. The indices were converted to the Mt. Wilson system of measurements and $\log R'_{\rm HK}$ values determined. A number of these stars had no previously derived activity indices. In addition we have also included the stars from Tinney et al. (2002) using our Mt. Wilson calibration. The radial-velocity instability (also known as *jitter*) level was determined for all 21 planet-host stars in our dataset. We find the jitter to be at a level considerably below the radial-velocity signatures in all but one of these systems. 19 stars from our sample were found to be active ($\log R'_{\rm HK} > $ -4.5) and thus have high levels of jitter. Radial-velocity analysis for planetary companions to these stars should precede with caution.

Key words:
stars: activity – stars: low-mass, brown dwarfs – planetary systems – ultraviolet: stars

1 INTRODUCTION

The Anglo-Australian Planet Search (AAPS) has been monitoring the radial-velocities of over 200 main sequence stars since January 1998 (e.g., Tinney et al. 2001). Radial-velocity searches are the cornerstones of current planet detections, giving rise to the bulk of the 171 extrasolar planets (Butler et al. 2006). However, dynamical activity in the stellar chromosphere (e.g., Queloz et al. 2001; Henry et al. 2002; Paulson et al. 2004) can mimic the radial-velocity signature of a planet. Indeed, it can be the primary source of uncertainty in attributing radial-velocity periodicities to a planetary companion, making the measurement of this activity in each planet search target star critical.

The level of activity associated with a target is most commonly determined by measuring the strength of the Calcium H and K lines in stellar spectra. The Mount Wilson HK Project (Duncan et al. 1991) has been utilising this technique since the mid-1960's for over 100 stars; currently the

project monitors over 400 dwarfs and giants. They have defined a $\log R'_{\rm HK}$ index, which various studies have shown to be a useful indicator of the level of radial-velocity instability (jitter) in F-K type dwarfs (e.g., Saar & Donahue 1997; Santos et al. 2002; Wright 2005). The Vienna-KPNO CaII H&K Survey (Strassmeier et al. 2000) has similar aims. Both these studies target northern hemisphere stars. There are no such studies conducted in the southern hemisphere that provide the continuous monitoring of activity that these projects in the north provide. Until recently (2006) there was only one large-scale activity analysis of solar-type stars in the southern hemisphere and this was provided by Henry et al. (1996) at the Cerro Tololo Inter-American Observatory (CTIO). Gray et al. (2006) have recently published the results of a spectroscopic survey conducted on stars earlier than M0 out to 40pc at the CTIO and the Stewart Observatory. These projects do not provide the long-term monitoring aspect of the Mount Wilson project, yet they provide us with a useful testbed to the conclusions

drawn in the north, whilst also providing an independent sample for statistical analysis.

When the AAPS list was drawn up, the vast majority of targeted stars were not on the activity list compiled by Henry et al. (1996). Henry et al. acknowledge that their primary sample of 650 stars south of -25° only comprise around 50% of the total number of solar-type stars in this region of the southern sky down to V∼9. Hence, to measure the chromospheric CaII HK core emission for all AAPS targets not in the Henry et al. catalogue we have taken spectra of 225 stars from the AAPS, a number of which had no previously derived activity indices. Also the majority of these objects are already being monitored by the AAPS for the presence of planetary companions, however some are being scrutinised as potential target candidates for an expansion of the target list.

2   OBSERVATIONS AND REDUCTION

Six nights of observations were taken over a period of four years and are listed in Tables 1 and 2. The observations were made using the University College London Echelle Spectrograph mounted on the 3.9-m Anglo-Australian Telescope (AAT), and followed the observing procedures described by Tinney et al. (2002). We used the EEV2 2048 x 4096 13.5-μm pixel detector, with a CaII HK quantum efficiency (QE) of ∼65%, for observations made on the nights 2001 August 04, 2002 July 20, 2003 July 21 and 2005 June 16. The CCD was spatially binned by two to give effective slit lengths of 11, 14, 23.5 and 17.5 pixels. The dispersion at the CaII HK lines is 0.02Å pixel^{-1}, giving resolutions of 3.5, 4, 6 and 4 pixels or 0.07, 0.08, 0.12 and 0.08Å. The remaining nights of observations were conducted on 2004 August 23 and 24 using the MIT and Lincoln Labs (MITTL3) 2048 x 4096 chip. The chip has relatively low QE (∼18%) around the HK line region, however as these are bright sources this presented no problems. The CCD setup was similar to the EEV2 chip giving effective slit lengths of 23.5 pixels. The dispersion was again similar to that of the EEV2 runs (0.02Å pixel^{-1}) giving a resolution of 4.5 pixels or 0.09Å.

225 F6-M5 dwarfs and sub-giants were observed in seeing ranging from 0.7-1.4 arcseconds through slits of sizes 1.0 x 3.5, 1.0 x 4.0 and 1.0 x 6.0 arcseconds. We have also included the observations in Tinney et al. (2002) to complete this catalogue. Exposure times ranged from 30 seconds to 900 seconds for the faintest objects. This provided signal-to-noise ratios per 0.02Å wavelength pixel of between 10 and 80. The target stars were taken from the AAPS target list and were supplemented by calibration stars taken from the Mount Wilson HK Project (Duncan et al. 1991). These are used to calibrate onto the Mount Wilson system of measurements. All calibration stars are listed in Table 1, along with their visual magnitudes, colours, spectral types and derived activity indices.

The reduction was accomplished using standard ECHOMOP protocols (Mills et al. 1996). Prior to the ECHOMOP procedure the files were prepared by performing a bias or overscan subtraction and rotating them to ECHOMOP's desired alignment. Each of the five orders (142 - 146) were then traced, clipped, flat fielded and the scattered light was removed. No sky subtraction was needed as the sky
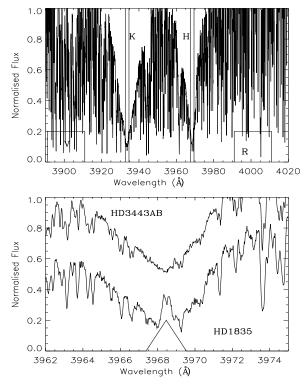

Figure 1. The Calcium H and K emission features, obtained at the AAT, for the star HD190248 (top panel). The R, V, H and K bandpasses are indicated for reference. The narrow features, other than H and K, are due to weak absorption lines not noise. The bottom panel shows the triangular bandpass used to integrate the flux for the CaII H feature. The calibration stars shown are HD3443AB (inactive: $\log R'_{\rm HK}$=-4.89) and HD1835 (active: $\log R'_{\rm HK}$=-4.45). Both have been offset from zero for clarity.

brightness around the CaHK lines is negligible compared to the brightness of our sources. Wavelength calibration was performed using ThAr arc spectra acquired for this purpose. The data acquired using the MITTL3 chip were then flux calibrated, as were the data from Tinney et al. (2002), in order to correct the blaze and inter-order sensitivity. This was accomplished using a measurement of the standard μ Col (Turnshek et al. 1990). None of the other three nights were flux calibrated. All spectra were then scrunched to a linear scale with bin widths of 0.02Å. All stars were then cross-correlated with an observation of HD216435 and the barycentric velocity for this star was applied, leaving a series of zero velocity spectra. Jones et al. (2002) have shown that HD216435 has a radial-velocity variation of 20ms^{-1} over a period of 1326 days (3.7 years). This is negligible when compared with the barycentric correction. The spectra were then normalised to the continuum region between 3991 and 4011Å, which represents the outer bandpass region (R) we used to acquire our desired activity index ($S_{\rm AAT}$).

To determine robust CaHK activity indices we employed four bandpasses centred around the calcium HK line cores. The V and R bandpasses both have square profiles with widths of 20Å and are centred on the continuum at 3901Å and 4001Å respectively. The K and H bandpasses have triangular profiles with FWHM's of 1.09Å and are centred on the cores themselves, at 3933.667Å and 3968.470Å
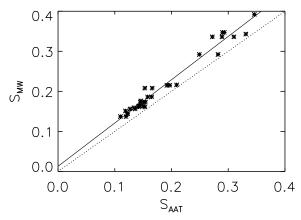
Figure 2. Calibration of the S_{AAT} index onto the S_{MW} system of measurements. The solid line represents a linear least-squares fit described by $S_{\mathrm{MW}} = (1.081 S_{\mathrm{AAT}}) + 0.013$, with a total RMS scatter of 0.014. The dotted line shows a 1:1 relationship.

respectively. Fig. 1 (upper) shows the final spectrum after the reduction procedure for the star HD190248. All four passbands are highlighted for reference. The H and K line cores are clearly evident. This star has a spectral type of G5IV-V. We find this star to be chromospherically quiet, with a final $\log R'_{\mathrm{HK}}$ of -5.03. The lower plot in Fig. 1 highlights the triangular bandpasses used to integrate the flux of the H line core. Two calibration stars are shown for reference, those are HD3443AB (top) and HD1835 (bottom), and both have been offset from zero for clarity. The stars are both main sequence stars and have spectral types of K1V and G3V respectively. The more active of the two (HD1835) exhibits some marked emission at the central core, whereas the inactive star (HD3443AB) has a deep central minima. It is these characteristics that allow accurate activity indices to be generated.

3 ANALYSIS

3.1 *S* Indices

Our spectra have been used to measure CaII HK emission (S_{MW}) indices (Duncan et al. 1991). This index is a measure of the ratio between the integrated flux in two triangular bandpasses (with FWHM's of 1.09Å) centred on the CaII H (3968.470 Å) and K (3933.664 Å) lines, against the integrated flux in two square 20Å continuum bandpasses at either side of the HK features, centred at 3901Å (V) and 4001Å (R). The Mt. Wilson (MT) Project determine this index individually each night using a specialised multi-channel photometer. S_{MW} is defined as:

$$S_{\mathrm{MW}} = \alpha \frac{N_{\mathrm{H}} + N_{\mathrm{K}}}{N_{\mathrm{R}} + N_{\mathrm{V}}} \qquad (1)$$

where N_i is the number of counts in each bandpass (where i=H, K, V and R) and α is a constant that is determined each night by the observation of standards.

Using the same methodology used to determine Eq. 1,

Tinney et al. (2002) have shown that the emission index for stars observed at the AAT (S_{AAT}) is given by:

$$S_{\mathrm{AAT}} = \frac{N_{\mathrm{H},1} + N_{\mathrm{H},2} + N_{\mathrm{K},1} + N_{\mathrm{K},2}}{2(N_{\mathrm{R}} + N_{\mathrm{V}})} \qquad (2)$$

Here the N_{HK} terms have two components. This is due to positioning of the echellogram, which causes both the H and K features to appear in two adjacent orders.

We used Eq. 2 to combine the integrated flux values from all bandpasses, giving us a set of S_{AAT} values we could use to calibrate onto the MW system of measurements. We have employed slightly different instrumental setups in our study and have observed our targets across a range of S/N ratios therefore we have included individual measurements for multiple objects in our calibrations. We have also chosen the most stable calibrators possible from Duncan et al. (1991), allowing us a better estimation of the variability error in our final activity index. Columns 3 and 4 of Duncan et al. (1991) give the minimum and maximum S indices obtained at Mt. Wilson. Over the course of one observing season the measured S index can vary on the level of ± 0.05, therefore selecting the most stable calibrators helps us reduce this uncertainty. Fig. 2 shows the least-squares fit used to calibrate onto S_{MW}. The calibration we employ (S_{AAT}) has a slope of 1.081 ± 0.001 and a zero-point offset of 0.013 ± 0.007. The RMS scatter about the fit is 0.014. This level of scatter is lower than the scatter found by Tinney et al. (2002) who also calibrated against stars from the CTIO study. Henry et al. (1996) employed a different approach to both the MW Project and our AAT analysis. They centred 4Å-wide square bandpasses on the HK line cores, compared to the 1.09Å triangular bandpasses employed at MW. When the bandpasses here are widened non-linear calibrations are needed to convert to the MW system of measurements. We suspect this leads to increased systematic errors in HK values. Indeed when we include all objects in this study with CTIO indices in our calibration we find a similar scatter to Tinney et al. (2002) of around 0.02.

Table 2 shows all derived S_{AAT} activity indices, after calibration onto the MW system of measurements, along with their one sigma photon-counting uncertainties. The table is split by epoch and there are a few objects with more than one measurement. In the majority of cases the photon-counting errors are an order of magnitude below that of the overall scatter from the calibration. In order to fully quantify all sources of error in the reduction procedure, such as scattered light removal, proper blaze removal, precise flux calibration etc, we used the stable star HD10700 (τ Ceti) as a proxy for the reduction errors. We have acquired three separate measurements of τ Ceti spanning a period of three years and due to the extremely small variation of $\sim 1\%$ (Baliunas et al. 1995) this represents a good indicator of the random errors in the reduction procedure. The standard deviation of the three measurements here is 3%, which is slightly lower than that of the Keck and Lick errors from Wright et al. (2004). However, we only have three separate measurements, which likely gives rise to a slightly lower estimation of the random errors. This 3% error should also be taken into account when quantifying the significance of any of the activity indices in Table 2.
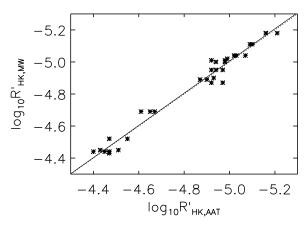
Figure 3. Derived $\log R'_{HK}$ chromospheric activities for the calibration stars on the AAPS target list. The solid line is a least-squares fit with a slope of 1.006 and a zero-point offset of 0.023. This result highlights the close relationship between the AAT and MW measurements. The dotted line is a direct 1:1 relationship.

3.2 $\log R'_{HK}$ Values

The S index provides an estimate of both the photospheric and chromospheric flux, and hence a combined CaII emission feature. In order to obtain actual activity values we have to concentrate on chromospheric flux, meaning photospheric effects have to be removed. This is accomplished by normalising the chromospheric emission to the bolometric luminosity of the star, and is most commonly designated by the $\log R'_{HK}$ parameter. We have followed Noyes et al. (1984) to convert all main sequence star values from S_{AAT} to $\log R'_{HK,AAT}$. We extrapolated the Noyes et al. conversion to include later spectral-types due to the lack of information on these stars. The Noyes et al. calibration is intended for stars in the colour range of B-V∼0.44-0.90, which means the final $\log R'_{HK}$ measurements of stars redder than 0.90 have a larger uncertainty than those in the calibration range. The derived values for the calibration stars are given in Table 1, along with the Duncan et al. $\log R'_{HK,MW}$ values. The values for all other objects are listed in Table 2. The Hipparcos B-V and visual magnitudes are shown in both tables for reference, and to highlight the photometric contribution to the S_{AAT} values.

In Fig. 3 we have plotted our $\log R'_{HK,AAT}$ values against the published values from Duncan et al. It can be seen from the gradient of the fit that there is good agreement with the MW data points. The gradient of the linear trend is 1.006±0.001 with an offset of 0.023±0.137. The RMS of the fit is 0.041, highlighting just how tight our values are to the published Mt. Wilson data. By using all the measurements in the calibration, and not just the means, we allow the error to include any variability and systematic effects. The dotted line in the figure shows a direct 1:1 relationship and it can be seen how close the $\log R'_{HK,MW}$ and $\log R'_{HK,AAT}$ are. We therefore employ no further calibration. Due to the inherently variable nature of stellar activity and errors in the reduction procedure, we believe the deduced RMS is a better measure of the overall error budget in each individual measurement.

4   DISCUSSION

Table 2 includes new and updated $\log R'_{HK}$ activities for 21 planetary systems from the AAPS. It must be noted that many more stars on this list probably have planetary systems that are still awaiting discovery or are below the detectability threshold of current radial-velocity surveys. We also include the observations from Tinney et al. (2002) using our new MW activity calibration. Most of these planetary hosts had previously derived $\log R'_{HK}$ values (e.g., Henry et al. 1996; Wright et al. 2004; Saffe et al. 2005). Gray et al. (2006) have recently completed the analysis of stars in the southern hemisphere for the NStars Project and the values in here are mostly in agreement with this work. However, the agreement with this work is not as tight as with Wright et al. (2004), most likely due to the different setups employed in this study as the Gray et al. approach used 4Å bandpasses, as opposed to the 1.09Å used in this work and the MW project. Indeed when we increase the widths of our bandpasses here, non-linear calibrations are needed onto the MW system.

Knowledge of the level of activity induced jitter in any radial-velocity measurement is essential to quantify the errors on a detected planetary fit. Jitter can vary on a timescale of days due to a number of different factors such as magnetic flux tube evolution, sub-photospheric convection, stellar oscillations and surface rotation of spots (Marcy et al. 2005) and can thus have a significant bearing on radial-velocity measurements. Therefore determining the jitter level of independent measurements allows one to generate a more precise velocity point and hence a more precise overall Keplerian fit.

The 21 planetary systems in this work have $\log R'_{HK}$ values ranging from -5.35 (HD27442) to -4.43 (HD22049). HD22049 (aka. Eps Eri) already had measurements taken at MW and they agree with our derived mean value of -4.43, confirming the high activity of the host star. Saar et al. (1998), Santos et al. (2000) and Wright (2005) have carried out studies probing the relationship between stellar activity and radial velocity jitter (σ'_{rv}). Wright provides an empirical estimate of jitter, culminating in a jitter metric (σ'_{rv}), which is a function of stellar evolution (for a full detailed description of the analysis, see Eqs. 1 - 7 Wright 2005). Applying this methodology, and using Hipparcos B-V, M_V and a T_{EFF} from Valenti & Fischer (2005), we find the jitter level for the most active planet-host star in our catalogue (HD22049) to be ∼5.7ms^{-1} with 20th and 80th percentiles of 4.6 and 9.5 ms^{-1} respectively (see Wright appendix for an explanation of percentiles). This low level of jitter for such an active star arises because the star is spectral type K. Jitter falls off at later spectral types allowing lower radial-velocity trends to be found around active K stars than F stars. The radial-velocity amplitude (K) for HD22049 is 19±1.7ms^{-1} (Hatzes et al. 2000). This level of velocity is significantly above our derived jitter. We therefore conclude that activity is not the source of the radial-velocity signature for HD22049.

Two other planet-host stars are shown to be quite active, both have $\log R'_{HK,AAT}$ values larger than Eps Eri. The first of these is HD13445 and it has a $\log R'_{HK,AAT}$ of -4.64. As this star is a K-dwarf the level of jitter it exhibits is not extremely high but it should be in the range 6-13ms^{-1}. The

planetary fit to this star has an amplitude of 380 ± 1ms^{-1} with a period of 15.78 days and from this a minimum mass of ~4M$_J$ was derived for the planet (Queloz et al. 2000). It is clear the jitter for this star is significantly lower than the observed radial-velocity measurements. The second of the two stars is HD17051 (ι Hor) and it has a log$R'_{HK,AAT}$ value of -4.59. Kürster et al. (2000) announced the detection of a planet with a minimum mass of 2.26M$_J$ and a period of 320.1 ± 2.1 days. The amplitude of the planetary fit is 67ms^{-1} with an RMS scatter of 27ms^{-1}. The internal errors were estimated to be 17ms^{-1} and they speculated the difference was activity induced, with a jitter of 20ms^{-1} making up this difference. Butler et al. (2001) obtained an RMS of 10.4ms^{-1} for this star using measurements made at the AAT and Saar et al. (1998) find a jitter of 10ms^{-1}, consistent with the AAT scatter. A further 10 measurements have been taken by Bulter et al. since 2001 over a period of 4 years and the current best-fit single-planet Keplerian has an RMS of 20ms^{-1}, consistent with the results from Kürster et al. (2000). We find a jitter range of 9-19ms^{-1}, which agrees well with observations and the higher end of this range can go a long way toward explaining the high level of scatter observed by Kürster et al. (2000) and Butler et al. (private communication).

17 out of the other 18 remaining planet-hosts objects are relatively inactive. These are HD142, HD2039, HD20782, HD23079, HD27442, HD30177, HD70642, HD73526, HD76700, HD102117, HD134987, HD142415, HD154857, HD169830, HD179949, HD216435 and HD216437. We find that the derived jitter value can not explain the observed stellar radial-velocity signal confirming the planetary hypothesis. However, the remaining star (HD10647) is spectral type F and we find the radial-velocity jitter is likely to be similar to the reported planetary signal. Mayor (2003) announced a best-fit Keplerian to the data with a K of 18 ± 1ms^{-1}, giving rise to a planet with a period of 1040 days (2.85 yrs) and a Msin$i$ of ~0.91 M$_J$. We find the log$R'_{HK,AAT}$ index to be -4.70. This relates to a jitter of ~11-23ms^{-1} at the 1-sigma level. This level of jitter is similar to the derived planetary signature. The star also exhibits a strong IR excess (Decin et al. 2000) which may be indicative of the presence of a disk. This also agrees well with the active nature of the star as this indicates the star is young. Mayor acknowledged the jitter phenomenon and by the use of a bisector analysis, they found no evidence for any periodic line profile variability. Jones et al. (2004) find only weak evidence for a planetary companion in the AAPS dataset for this object. However, four additional measurements have been taken at the AAT for this star over a period of 2 years. The current best-fit Keplerian has a period of 2.73 years with an amplitude of 17.9ms^{-1}. The RMS to the fit is 8.9ms^{-1}. This signature is in agreement with the signal announced by Mayor (2003), however with a false alarm probability of 0.25 more data points will be needed to obtain robust planetary parameters.

4.1 logR'_{HK} Distribution:-

Fig. 4 shows the distribution of stellar activity for 225 stars on the AAPS target list. The selection criteria for the list itself targets more evolved stars, and as such the inactive peak was expected. We see the indication of a possible binomial
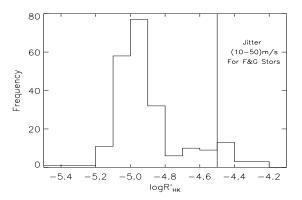

Figure 4. A histogram of the logR'_{HK} activity index distribution for the stars on the AAPS target list. It is clear that the majority of the stars observed by the AAPS are inactive, with the peak residing at values below -4.90. The solid vertical line bounds the region inhabited by very active stars. The lower limit radial-velocity jitter range is shown for F and G stars in this region.

distribution in activity with peaks centred at -4.95 and -4.45. This result has been found before in both the northern and southern hemispheres (e.g., Vaughan & Preston 1980; Henry et al. 1996).

There are a number of highly active (logR'_{HK} > -4.5) stars on this list. For the assessment of highly active stars we use the Santos et al. (2000) jitter relation (see Eqs. 2 - 4 from Santos et al. 2000), as the Wright model is out of range for some of our active stars. The vertical solid line in Fig. 4 represents the lower boundary of these active stars. There are 19 stars in this region. Since the R'_{HK}-σ'(Vr) relation decreases with spectral type, the jitter values of half of these are closer to the lower end of this range, as 9 of these stars are K-dwarfs. However, all are expected to have jitter values in excess of ~7ms^{-1}, therefore the low-amplitude radial-velocity signatures of companions must be treated with care. Also two of the active set are M-dwarfs, and with B-V colours >1.5 they are outside the model limits for jitter determination. Wright (2005) shows that M-type stars statistically exhibit higher jitter levels than F,G,K-type stars. Therefore, we expect these two active M stars to exhibit high levels of jitter.

Analysis of the remaining F and G-type stars, HD1835, HD11131, HD13246, HD19632, HD88201, HD90712, HD129060 and HD152391 show these are likely to have jitter values around ~10-30ms^{-1}. HD1835 and HD11131 were used as calibrators, and both the MW and CTIO studies have found these to be highly active. This level of jitter has already proven sufficient to mimic a planetary companion (e.g., Queloz et al. 2001; Henry et al. 2002). It must be noted that the logR'_{HK} > -4.5 is a somewhat arbitrary cut-off. An F-type star, such as HD16673, with a logR'_{HK} value of -4.64, still provides a jitter range of around: σ ~11-24ms^{-1}. Therefore, it is necessary to take great care when dealing with radial-velocity amplitudes for all F-type stars >-4.70. Indeed the two active F-type stars (HD13246 and HD129060) exhibit extremely high levels of jitter. Having logR'_{HK} values of -4.38 and -4.41 respectively, they exhibit jitter of around ~17-40ms^{-1}. This level of jitter puts serious limitations on the potential for planet discoveries around these stars. The AAPS baseline is

8 years and even giant planets with orbital periods longer than this do not generate large radial-velocity amplitudes. For example, Jupiter, with a semimajor axis of 5.2AU, induces a radial-velocity motion of $\sim$12ms^{-1} on the Sun over a 12 year period. The jitter level exhibited by both these stars could serve to mask the planetary signature of an orbiting Jupiter even once the baseline is sufficient to detect them.

Due to the variable nature of stellar activity, in particular when dealing with active stars, it is important to obtain multi-epoch activity indices. This will allow planet searches to state categorically that the jitter-level is significantly lower than any companion's periodic radial-velocity signature. It is even more essential in the southern hemisphere, where no such program yet exists. We have obtained more than one measurement for a small number of our stars, but with a maximum of three observations, we are still limited by a lack of data. At MW a number of measurements are obtained of the same object over an observing season. The difference in $\log R'_{HK}$-index over one season can change at the level of $\sim \pm 0.2$ (see Duncan et al. 1991 Table 1 column 5). This variation was recorded using a single well defined setup (e.g., HD16673: 202 measurements: -4.66 $\leqslant \log R'_{HK} \leqslant$ -4.82). Another example would be our own parent star. The $\log R'_{HK}$-index of the Sun varies from its typical value of $\sim$-5.10 to -4.96 during the Solar minimum (Wright et al. 2004). This level of discrepancy highlights the difficulty when attempting to calibrate between systems and when trying to fully quantify activity. This is why gaining multiple measurements using a well defined standard setup is essential.

Time series analysis also allows other avenues of study to be undertaken. Stellar ages and rotation periods can be empirically estimated using $\log R'_{HK}$ relationships. For instance the age-chromospheric activity relation of Soderblom et al. (1991), most recently updated to its current form by Baliunas et al. (1995) and taken from Wright (2005) is given by:

$$log[t(\text{yr})] = -0.0522 R_5^3 + 0.4085 R_5^2 - 1.334 R_5 + 10.725 \quad (3)$$

here $R_5 = 10^5 R'_{HK}$ and R'_{HK} represents the activity level for a solar-type star averaged over many stellar activity cycles. The more observations one obtains, the closer one gets to the actual age derived from this relationship. This is because taking multiple measurements allows a better determination of the mean activity index for main sequence stars. Using the Sun's variability range from above ($\sim$-5.10 to -4.96) causes measurements of the solar age to differ by several Gyrs (e.g. 7.92 - 4.93 Gyrs). Variability knowledge is essential to obtain reliable age and rotation estimates of stars.

Acknowledgements

REFERENCES

Baliunas S. L., Donahue R. A., Soon W., Gilliland R., Soderblom D. R., 1995, BAAS, 27, 839

Butler R. P., Tinney C. G., Marcy G. W., Jones H. R. A., Penny A. J., Apps K., 2001, ApJ, 555, 410

Butler R. P., Wright J. T., Marcy G. W., Fischer D. A., Vogt S. S., Tinney C. G., Jones H. R. A., Carter B. D., Johnson A. J., McCarthy C., Penny A. J., 2006, preprint

Decin G., Dominik C., Malfait K., Mayor M., Waelkens C., 2000, A&A, 357, 533

Duncan D. K., Vaughan A. H., Wilson O. C., Preston G. W., Frazer J., Lanning H., Misch A., Mueller J., Soyumer D., Woodard L., Baliunas S. L., Noyes R. W., Hartmann L. W., Porter A., Zwaan C., Middelkoop F., Rutten R. G. M., Mihalas D., 1991, ApJS, 76, 383

Gray R. O., Corbally C. J., Garrison R. F., McFadden M. T., Bubar E. J., McGahee C. E., O'Donoghue A. A., Knox E. R., 2006, AJ, 132, 161

Hatzes A. P., Cochran W. D., McArthur B., Baliunas S. L., Walker G. A. H., Campbell B., Irwin A. W., Yang S., Kürster M., Endl M., Els S., Butler R. P., Marcy G. W., 2000, ApJL, 544, L145

Henry G. W., Donahue R. A., Baliunas S. L., 2002, ApJL, 577, L111

Henry T. J., Soderblom D. R., Donahue R. A., Baliunas S. L., 1996, AJ, 111, 439

Jones H. R. A., Butler R. P., Tinney C. G., Marcy G. W., McCarthy C., Penny A. J., Carter B. D., 2004, Astronomical Society of the Pacific Conference Series, 321, 298

Jones H. R. A., Paul Butler R., Marcy G. W., Tinney C. G., Penny A. J., McCarthy C., Carter B. D., 2002, MNRAS, 337, 1170

Kürster M., Endl M., Els S., Hatzes A. P., Cochran W. D., Döbereiner S., Dennerl K., 2000, A&A, 353, L33

Marcy G. W., Butler R. P., Vogt S. S., Fischer D. A., Henry G. W., Laughlin G., Wright J. T., Johnson J. A., 2005, ApJ, 619, 570

Mayor M., 2003, Astronomical Society of the Pacific Conference Series, 321

Mills D., Webb J., Clayton M., 1996, Starlink, 152, 1

Noyes R. W., Hartmann L. W., Baliunas S. L., Duncan D. K., Vaughan A. H., 1984, ApJ, 279, 763

Paulson D. B., Cochran W. D., Hatzes A. P., 2004, AJ, 127, 3579

Queloz D., Henry G. W., Sivan J. P., Baliunas S. L., 2001, A&A, 379, 279

Queloz D., Mayor M., Weber L., Blécha A., Burnet M., Confino B., Naef D., Pepe F., Santos N., Udry S., 2000, A&A, 354, 99

Saar S. H., Butler R. P., Marcy G. W., 1998, ApJL, 498, L153

Saar S. H., Donahue R. A., 1997, ApJ, 485, 319

Saffe C., Gómez M., Chavero C., 2005, A&A, 443, 609

Santos N. C., Mayor M., Naef D., Pepe F., Queloz D., Udry S., Blecha A., 2000, A&A, 361, 265

Santos N. C., Mayor M., Naef D., Pepe F., Queloz D., Udry S., Burnet M., Clausen J. V., Helt B. E., Olsen E. H., Pritchard J. D., 2002, A&A, 392, 215

Soderblom D. R., Duncan D. K., Johnson D. R. H., 1991, ApJ, 375, 722

Strassmeier K., Washuettl A., Granzer T., Scheck M., Weber M., 2000, A&AS, 142, 275

Tinney C. G., Butler R. P., Marcy G. W., Jones H. R. A., Penny A. J., Vogt S. S., Apps K., Henry G. W., 2001, ApJ, 551, 507

Table 1. S and $\log R'_{HK}$ activity values for all stars used to calibrate onto the Mt. Wilson system of measurements. <u>Column Headings:-</u> HD Number:- Henry Draper catalogue identifiers. Johnson B-V, V and Spec Type all taken from Hipparcos. S_{AAT} *after* calibration onto the Mt. Wilson system. S_{MW} is the Mt. Wilson index used to perform this calibration, taken from column 5 of Table 1 and columns 4-7 of Table 3 from Duncan et al. (1991). $\log R'_{HK,MW}$ are derived from (Duncan et al. 1991). Note: the photon-counting errors are indicative only, a random error of $\gtrsim 3\%$ must be taken into account in all instances. This error was estimated from measurements of τ Ceti.

.

HD	B-V	V	Spec Type	S_{AAT}	S_{MW}	$\log R'_{HK,AAT}$	$\log R'_{HK,MW}$
Calibrators							
HD1835	0.659	6.39	G3V	0.330±0.002, 0.326±0.002, 0.371±0.002	0.347	-4.47, -4.47, -4.40	-4.44
HD3443AB	0.715	5.57	K1V	0.184±0.001, 0.191±0.001	0.186	-4.87, -4.90	-4.89
HD3795	0.718	6.14	G3/G5V	0.150±0.001, 0.157±0.001, 0.160±0.001	0.156	-5.02, -5.03, -5.07	-5.04
HD9562	0.639	5.75	G2IV	0.145±0.001, 0.146±0.001	0.144	-5.09, -5.10	-5.11
HD10700	0.727	3.49	G8V	0.169±0.001, 0.176±0.001, 0.179±0.001	0.173	-4.92, -4.94, -4.97	-4.95
HD11131	0.654	6.72	G0	0.307±0.002, 0.325±0.002, 0.348±0.002	0.336	-4.43, -4.47, -4.51	-4.45
HD16673	0.524	5.79	F6V	0.221±0.001, 0.225±0.001, 0.239±0.002	0.215	-4.61, -4.65, -4.67	-4.69
HD23249	0.915	3.52	K0IV	0.132±0.001, 0.142±0.001, 0.142±0.001	0.137	-5.16, -5.16, -5.21	-5.18
HD26965	0.820	4.43	K1V	0.178±0.001, 0.192±0.001	0.208	-4.92, -4.97	-4.87
HD30495	0.632	5.49	G3V	0.282±0.002, 0.317±0.002	0.292	-4.47, -4.55	-4.52
HD81809	0.642	5.38	G2V	0.170±0.001	0.160	-4.93	-4.90
HD115617	0.709	4.74	G5V	0.166±0.001, 0.178±0.001	0.161	-4.92, -4.98	-5.01
HD152391	0.749	6.65	G8V	0.387±0.003, 0.458±0.003	0.392	-4.36, -4.45	-4.44
HD158614	0.715	5.31	G8IV-V	0.167±0.001, 0.175±0.001	0.163	-4.94, -4.98	-5.00
HD219834AC	0.787	5.20	G6/G8IV	0.169±0.001	0.164	-4.99	-5.02

Tinney C. G., McCarthy C., Jones H. R. A., Butler R. P.,
 Carter B. D., Marcy G. W., Penny A. J., 2002, MNRAS,
 332, 759

Turnshek D. A., Bohlin R. C., Williamson R. L., Lupie
 O. L., Koornneef J., Morgan D. H., 1990, AJ, 99, 1243

Valenti J. A., Fischer D. A., 2005, ApJS, 159, 141

Vaughan A. H., Preston G. W., 1980, PASP, 92, 385

Wright J. T., 2005, PASP, 117, 657

Wright J. T., Marcy G. W., Butler R. P., Vogt S. S., 2004,
 ApJS, 152, 261

Table 2. S_{AAT} and $\log R'_{\mathrm{HK,AAT}}$ for stars on or under consideration for the AAPS. Column Headings:- HD Number:- Henry Draper catalogue identifiers (numbers with associated asterisks (*) highlight planet bearing stars). Johnson B-V, V and Spec Type all taken from the Hipparcos catalogue. S_{AAT}:- the AAT activity index *after* calibration onto the Mt. Wilson system of measurements. For objects with multiple measurements we have included all the individual indices. $\log R'_{\mathrm{HK,AAT}}$:- final activity values generated following the Noyes et al. (1984) methodology. Note: the photon-counting errors are indicative only, a random error of $\gtrsim 3\%$ must be taken into account in all instances. This error was estimated from measurements of τ Ceti.

HD	B-V	V	Spec Type	S_{AAT}	$\log R'_{\mathrm{HK,AAT}}$
Measurements					
2001 August 04th					
*HD142	0.519	5.70	G1IV	0.161±0.001	-4.95
*HD2039	0.656	9.00	G2/G3IV/V	0.180±0.001	-4.89
HD2587	0.748	8.46	G6V	0.152±0.001	-5.07
HD3823	0.564	5.89	G1V	0.160±0.001	-4.97
HD6735	0.567	7.01	F8V	0.173±0.001	-4.89
HD7199	0.849	8.06	K0IV/V	0.177±0.001	-4.99
HD7570	0.571	4.97	F8V	0.166±0.001	-4.93
HD9280	0.760	8.03	G5	0.148±0.001	-5.09
HD10180	0.629	7.33	G1V	0.165±0.001	-4.96
HD10647	0.551	5.52	F8V	0.213±0.001	-4.70
HD11112	0.637	7.13	G4V	0.158±0.001	-5.00
*HD13445	0.812	6.12	K0V	0.302±0.002	-4.64
HD16417	0.653	5.78	G1V	0.148±0.001	-5.08
*HD17051	0.561	5.40	G3IV	0.249±0.002	-4.59
HD18907	0.794	5.88	G8/K0V	0.147±0.001	-5.11
HD19632	0.678	7.29	G3/G5V	0.369±0.002	-4.41
HD20029	0.561	7.05	F7V	0.156±0.001	-4.99
HD20201	0.584	7.27	G0V	0.178±0.001	-4.87
HD20766	0.641	5.53	G2V	0.270±0.002	-4.58
*HD20782	0.630	7.36	G3V	0.186±0.001	-4.85
HD20807	0.600	5.24	G1V	0.184±0.001	-4.84
HD22104	0.679	8.32	G3V	0.155±0.001	-5.04
*HD23079	0.583	7.12	F8/G0V	0.163±0.001	-4.95
HD23127	0.690	8.58	G2V	0.162±0.001	-5.00
HD23484	0.870	6.99	K1V	0.508±0.003	-4.43
HD24112	0.560	7.24	F8V	0.155±0.001	-5.00
HD25587	0.543	7.40	F7V	0.164±0.001	-4.93
HD25874	0.667	6.74	G5IV-V	0.169±0.001	-4.95
HD26754	0.551	7.16	F7/F8V	0.159±0.001	-4.97
*HD27442	1.078	4.44	K2IV	0.129±0.001	-5.35
HD28255	0.659	6.28	G4V	0.188±0.001	-4.85
*HD30177	0.773	8.41	G8V	0.152±0.001	-5.08
HD30876	0.901	7.49	K2V	0.468±0.003	-4.51
HD31527	0.606	7.49	G2V	0.172±0.001	-4.91
HD36108	0.590	6.78	G3V	0.155±0.001	-5.01
HD38283	0.584	6.69	G0/G1V	0.161±0.001	-4.97
HD38382	0.580	6.34	F8/G0V	0.167±0.001	-4.93
HD38973	0.594	6.63	G2V	0.161±0.001	-4.97
HD40307	0.935	7.17	K3V	0.265±0.002	-4.83
HD202628	0.637	6.75	G5V	0.257±0.002	-4.61
HD204385	0.596	7.14	G0IV	0.166±0.001	-4.94
HD204961	1.521	8.66	M1V	0.985±0.007	-5.10
HD205390	0.879	7.14	K2V	0.426±0.003	-4.53
HD205536	0.755	7.07	G8V	0.164±0.001	-5.01
HD209268	0.564	6.88	F7V	0.156±0.001	-4.99
HD211317	0.650	7.26	G5III/IV	0.156±0.001	-5.02
HD212168	0.599	6.12	G3IV	0.161±0.001	-4.97
*HD216437	0.660	6.04	G4IV-V	0.155±0.001	-5.03
HD217987	1.483	7.35	M2/M3V	1.081±0.007	-5.01
HD222237	0.989	7.09	K3V	0.296±0.002	-4.84
HD222335	0.802	7.18	K1V	0.238±0.002	-4.77
2002 July 20th					
GL551	1.807	11.01	M5Ve	10.686±0.072	-4.28
GL729	1.510	10.37	M3.5Ve	6.188±0.042	-4.29
HD1273	0.655	6.84	G2V	0.192±0.001	-4.83
HD1581	0.576	4.23	F9V	0.167±0.001	-4.92

HD2071	0.681	7.27	G8IV	0.184±0.001	-4.88
HD5133	0.936	7.15	K2V	0.464±0.003	-4.56
HD5562	0.808	7.17	G8IV	0.147±0.001	-5.11
HD7570	0.571	4.97	F8V	0.159±0.001	-4.97
HD7693	1.000	7.22	K2V	0.655±0.004	-4.48
HD8581	0.569	6.85	F8V	0.152±0.001	-5.03
HD9540	0.766	6.97	K0V	0.365±0.002	-4.49
HD12042	0.487	6.10	F8V	0.161±0.001	-4.94
HD13246	0.544	7.50	F8V	0.341±0.002	-4.38
HD17925	0.862	6.05	K1V	0.674±0.004	-4.29
*HD22049	0.881	3.72	K2V	0.480±0.003	-4.47
HD23456	0.511	6.97	G1V	0.166±0.001	-4.91
HD27274	1.115	7.64	K5V	0.416±0.003	-4.86
HD30295	0.812	8.86	K0/K1V	0.142±0.001	-5.13
HD31827	0.770	8.26	G8IV	0.149±0.001	-5.09
HD33811	0.765	8.71	G8IV/V	0.164±0.001	-5.01
HD38110	0.696	8.18	G5	0.159±0.001	-5.02
HD38393	0.481	3.59	F7V	0.167±0.001	-4.90
HD40307	0.935	7.17	K3V	0.255±0.002	-4.85
HD84117	0.534	4.93	G0V	0.158±0.001	-4.97
HD85512	1.156	7.67	K5V	0.312±0.002	-5.05
HD85512	1.156	7.67	K5V	0.383±0.002	-4.96
HD85683	0.546	7.34	F8V	0.165±0.001	-4.93
HD85683	0.546	7.34	F8V	0.168±0.001	-4.91
HD85683	0.546	7.34	F8V	0.168±0.001	-4.91
HD97998	0.626	7.36	G5V	0.187±0.001	-4.84
HD101581	1.064	7.77	K5V	0.500±0.003	-4.70
HD101805	0.528	6.48	G1V	0.160±0.001	-4.95
*HD102117	0.721	7.47	G6V	0.158±0.001	-5.03
HD103026	0.554	5.85	F8V	0.150±0.001	-5.04
HD103493B	0.646	6.70	G5V	0.194±0.001	-4.82
HD103975	0.527	6.76	G0V	0.162±0.001	-4.94
HD105328	0.613	6.72	G2V	0.161±0.001	-4.97
HD106453	0.711	7.47	K0/K1V	0.319±0.002	-4.52
HD106869	0.574	6.81	G1V	0.162±0.001	-4.96
HD110810	0.937	7.82	K3V	0.623±0.004	-4.42
HD112019	0.520	7.69	G0V	0.165±0.001	-4.92
HD113027	0.569	7.56	G2V	0.189±0.001	-4.81
HD114260	0.718	7.36	G6V	0.173±0.001	-4.95
HD114613	0.693	4.85	G3V	0.157±0.001	-5.03
HD114613	0.693	4.85	G3V	0.157±0.001	-5.03
HD115585	0.742	7.43	G6IV-V	0.152±0.001	-5.07
HD117105	0.583	7.20	G1V	0.167±0.001	-4.93
HD117939	0.669	7.29	G3V	0.181±0.001	-4.89
HD118475	0.618	6.97	G2/G3IV/V	0.166±0.001	-4.95
HD118972	0.855	6.92	K1V	0.503±0.003	-4.42
HD120780	0.891	7.37	K1V	0.264±0.002	-4.79
HD122862	0.581	6.02	G1V	0.157±0.001	-4.99
HD124584	0.590	7.29	G0/G1V	0.160±0.001	-4.98
HD125072	1.017	6.66	K3V	0.283±0.002	-4.89
HD125370	1.095	8.53	K0III	0.179±0.001	-5.21
HD128674	0.672	7.39	G5V	0.188±0.001	-4.86
HD129060	0.553	6.99	F7V	0.330±0.002	-4.41
HD134606	0.740	6.86	G5IV	0.157±0.001	-5.04
*HD134987	0.691	6.47	G5V	0.155±0.001	-5.04
HD136352	0.639	5.65	G2V	0.176±0.001	-4.90
HD140785	0.660	7.38	G5V	0.154±0.001	-5.04
HD140901	0.715	6.01	G6IV	0.256±0.002	-4.66
*HD142415	0.621	7.33	G1V	0.235±0.002	-4.66
HD143114	0.606	7.34	G3V	0.171±0.001	-4.92
HD144009	0.714	7.23	G8V	0.193±0.001	-4.86
HD144628	0.856	7.11	K3V	0.193±0.001	-4.94
HD145417	0.815	7.53	K0V	0.210±0.001	-4.86
HD145809	0.617	6.68	G3V	0.154±0.001	-5.02
HD146481	0.642	7.09	G4V	0.160±0.001	-4.99
HD147723	0.625	5.40	G0IV	0.147±0.001	-5.08
HD147723	0.625	5.40	G0IV	0.159±0.001	-4.99
HD149612	0.616	7.01	G3V	0.179±0.001	-4.87

HD150474	0.780	7.16	G8V	0.148±0.001	-5.10
HD151337	0.901	7.38	K0V	0.147±0.001	-5.13
HD152311	0.685	5.86	G5IV	0.150±0.001	-5.07
HD153075	0.581	6.99	G0V	0.172±0.001	-4.90
HD154577	0.889	7.38	K0V	0.245±0.002	-4.82
*HD154857	0.699	7.24	G5V	0.154±0.001	-5.05
HD155918	0.607	7.00	G2V	0.175±0.001	-4.89
HD155974	0.479	6.09	F6V	0.159±0.001	-4.95
HD156274	0.764	5.47	M0V	0.176±0.001	-4.95
HD157060	0.541	6.42	F8V	0.161±0.001	-4.95
HD159868	0.714	7.24	G5V	0.171±0.001	-4.96
HD162396	0.523	6.19	F8V	0.155±0.001	-4.98
HD162521	0.451	6.36	F8V	0.227±0.001	-4.63
HD163272	0.614	7.39	G2/G3V	0.163±0.001	-4.96
HD165269	0.611	7.29	G1V	0.170±0.001	-4.92
HD166553	0.599	7.27	G1/G2V	0.157±0.001	-5.00
HD168060	0.759	7.34	G5V	0.148±0.001	-5.10
*HD169830	0.517	5.90	F8V	0.151±0.001	-5.02
HD171990	0.593	6.39	G2V	0.150±0.001	-5.05
HD179140	0.627	7.23	G2V	0.158±0.001	-5.00
*HD179949	0.548	6.25	F8V	0.198±0.001	-4.76
HD183877	0.675	7.14	K0	0.183±0.001	-4.88
HD184509	0.557	6.74	G1V	0.174±0.001	-4.88
HD188641	0.626	7.34	G2V	0.159±0.001	-5.00
HD190248	0.751	3.55	G5IV-V	0.160±0.001	-5.03
HD191408	0.868	5.32	K2V	0.195±0.001	-4.94
HD191849	1.431	7.97	M0V	1.630±0.011	-4.76
HD192310	0.878	5.73	K3V	0.204±0.001	-4.92
HD192865	0.558	6.91	F8V	0.158±0.001	-4.97
HD193193	0.594	7.20	G2V	0.165±0.001	-4.95
HD196068	0.640	7.18	G5V	0.150±0.001	-5.06
HD196378	0.544	5.11	F8V	0.158±0.001	-4.97
HD196390	0.626	7.33	G3V	0.203±0.001	-4.78
HD196800	0.607	7.21	G1/G2V	0.162±0.001	-4.97
HD202457	0.689	6.60	G5V	0.161±0.001	-5.00
HD202560	1.397	6.69	M1/M2V	0.993±0.007	-4.93
HD203985	0.876	7.49	K0V	0.190±0.001	-4.96
HD204287	0.663	7.33	G3V	0.154±0.001	-5.04
HD206395	0.559	6.67	G0IV	0.162±0.001	-4.95
HD209100	1.056	4.69	K5V	0.450±0.003	-4.74
HD210272	0.663	7.22	G3V	0.152±0.001	-5.05
HD213042	1.080	7.65	K4V	0.325±0.002	-4.92
*HD216435	0.621	6.03	G3IV	0.157±0.001	-5.01
HD216803	1.094	6.48	K4Vp	0.856±0.006	-4.51
HD219048	0.733	6.90	G5V	0.161±0.001	-5.02
HD221420	0.681	5.82	G2V	0.142±0.001	-5.13
HD222668	0.835	7.35	G8IV/V	0.150±0.001	-5.09
HD224619	0.741	7.47	G8V	0.184±0.001	-4.91
HD225213	1.462	8.56	M2V	0.383±0.002	-5.43
2003 April 21st					
HD4447	0.908	8.78	K0	0.157±0.001	-5.10
HD30876	0.901	7.49	K2V	0.393±0.003	-4.59
HD42902	0.623	8.92	G2/G3V	0.148±0.001	-5.07
HD44821	0.663	7.37	K0/1V	0.319±0.002	-4.49
HD44821	0.663	7.37	K0/1V	0.322±0.002	-4.48
HD45701	0.660	6.45	G3III/IV	0.157±0.001	-5.02
HD52447	0.605	8.38	G0V	0.148±0.001	-5.06
HD52447	0.605	8.38	G0V	0.149±0.001	-5.06
HD55693	0.660	7.17	G1V	0.164±0.001	-4.98
HD55720	0.705	7.50	G6V	0.166±0.001	-4.98
HD56560	0.737	7.33	G6IV/V	0.143±0.001	-5.12
HD59468	0.694	6.72	G5IV-V	0.162±0.001	-5.00
HD61686	0.693	8.54	G3V	0.136±0.001	-5.18
HD61686	0.693	8.54	G3V	0.144±0.001	-5.12
HD65907A	0.573	5.59	G2V	0.173±0.001	-4.89
HD67199	0.872	7.18	K1V	0.336±0.002	-4.64
HD67556	0.548	7.30	F8V	0.175±0.001	-4.87

HD69655	0.579	6.63	G1V	0.165±0.001	-4.94
*HD70642	0.692	7.17	G8:III	0.167±0.001	-4.97
*HD70642	0.692	7.17	G8:III	0.168±0.001	-4.97
HD70889	0.600	7.09	G0V	0.237±0.002	-4.64
HD72769	0.745	7.22	K1IV	0.147±0.001	-5.10
HD73121	0.578	6.44	G1V	0.169±0.001	-4.92
HD74868	0.567	6.56	G3IV	0.159±0.001	-4.98
*HD76700	0.745	8.16	G8V	0.130±0.001	-5.22
*HD76700	0.745	8.16	G8V	0.136±0.001	-5.18
HD78429	0.664	7.31	G5V	0.202±0.001	-4.80
HD80635	0.729	8.80	G3IV	0.135±0.001	-5.18
HD80635	0.729	8.80	G3IV	0.141±0.001	-5.14
HD80913	0.556	7.49	F6V	0.152±0.001	-5.02
HD88201	0.558	7.45	G0V	0.357±0.002	-4.36
HD90712	0.585	7.52	G2/G3V	0.388±0.003	-4.32
HD109200	0.836	7.13	K0V	0.189±0.001	-4.94

2004 August 23$^{\mathrm{rd}}$ & 24$^{\mathrm{th}}$

HD7442	0.587	7.17	F8/G0V	0.151±0.001	-5.04
HD13578	0.620	7.50	G3IV	0.156±0.001	-5.01
HD16427	0.568	6.84	F8V	0.164±0.001	-4.94
HD17925	0.862	6.05	K1V	0.699±0.005	-4.27
HD21626	0.501	6.73	G0IV	0.147±0.001	-5.05
*HD22049	0.881	3.72	K2V	0.563±0.004	-4.39
HD22924	0.552	6.94	F8/G0V	0.152±0.001	-5.02
HD23308	0.522	6.50	F8V	0.250±0.002	-4.57
HD28454	0.470	6.10	F8V	0.160±0.001	-4.95
HD31975	0.521	6.28	F8V	0.169±0.001	-4.90
HD32820	0.528	6.30	F8V	0.159±0.001	-4.96
HD33473	0.662	6.75	G3V	0.162±0.001	-4.99
HD34606	1.014	8.92	G5	0.168±0.001	-5.14
HD38393	0.481	3.59	F7V	0.158±0.001	-4.96
*HD142415	0.621	7.33	G1V	0.260±0.002	-4.59
HD146481	0.642	7.09	G4V	0.181±0.001	-4.88
HD147722	0.625	5.40	G0	0.168±0.001	-4.94
HD147722	0.625	5.40	G0	0.181±0.001	-4.87
HD149612	0.616	7.01	G3V	0.205±0.001	-4.76
HD150474	0.780	7.16	G8V	0.166±0.001	-5.00
HD151337	0.901	7.38	K0V	0.158±0.001	-5.09
HD153075	0.581	6.99	G0V	0.195±0.001	-4.79
HD154577	0.889	7.38	K0V	0.252±0.002	-4.81
*HD154857	0.699	7.24	G5V	0.173±0.001	-4.94
HD155974	0.479	6.09	F6V	0.162±0.001	-4.93
HD179140	0.627	7.23	G2V	0.175±0.001	-4.90
*HD179949	0.548	6.25	F8V	0.209±0.001	-4.72
HD183877	0.675	7.14	K0	0.194±0.001	-4.84
HD188641	0.626	7.34	G2V	0.171±0.001	-4.92
HD192310	0.878	5.73	K3V	0.238±0.002	-4.83
HD192865	0.558	6.91	F8V	0.164±0.001	-4.94
HD193193	0.594	7.20	G2V	0.186±0.001	-4.83
HD196068	0.640	7.18	G5V	0.160±0.001	-5.00
HD196378	0.544	5.11	F8V	0.162±0.001	-4.95
HD196390	0.626	7.33	G3V	0.243±0.002	-4.64
HD196800	0.607	7.21	G1/G2V	0.160±0.001	-4.98
HD202560	1.397	6.69	M1/M2V	1.076±0.007	-4.89
HD202560	1.397	6.69	M1/M2V	1.111±0.007	-4.88
HD203985	0.876	7.49	K0V	0.188±0.001	-4.96
HD203985	0.876	7.49	K0V	0.191±0.001	-4.95
HD204287	0.663	7.33	G3V	0.164±0.001	-4.97
HD207129	0.601	5.57	G2V	0.184±0.001	-4.85
HD212330	0.665	5.31	F9V	0.164±0.001	-4.98
*HD216435	0.621	6.03	G3IV	0.164±0.001	-4.96
HD216803	1.094	6.48	K4Vp	1.084±0.007	-4.41
HD219048	0.733	6.90	G5V	0.162±0.001	-5.01
HD222668	0.835	7.35	G8IV/V	0.160±0.001	-5.05
HD224619	0.741	7.47	G8V	0.192±0.001	-4.88

2005 June 16th					
HD56957	0.701	7.57	G3V	0.148±0.001	-5.09
HD63685	0.758	7.38	G5V	0.157±0.001	-5.04
HD67556	0.548	7.30	F8V	0.196±0.001	-4.77
HD69655	0.579	6.63	G1V	0.176±0.001	-4.88
*HD70642	0.692	7.17	G8:III	0.175±0.001	-4.93
HD72769	0.745	7.22	K1IV	0.161±0.001	-5.02
*HD73526	0.737	8.99	G6V	0.154±0.001	-5.05
HD74868	0.567	6.56	G3IV	0.165±0.001	-4.93
*HD76700	0.745	8.16	G8V	0.160±0.001	-5.02
HD80913	0.556	7.49	F6V	0.166±0.001	-4.93
HD94340	0.645	7.02	G3/G5V	0.293±0.002	-4.53
HD95456	0.527	6.06	F8V	0.168±0.001	-4.91
HD142022	0.790	7.70	K0V	0.166±0.001	-5.01